Measurement of the ^{3}He Spin-Structure Functions and of Neutron (^{3}He) Spin-Dependent Sum Rules at $0.035 \leq Q^2 \leq 0.24$ GeV^2

V. Sulkosky,[1,2,3] J. T. Singh,[3] C. Peng,[4] J.-P. Chen,[2] A. Deur*,[3,2] S. Abrahamyan,[5] K. A. Aniol,[6] D. S. Armstrong,[1] T. Averett,[1] S. L. Bailey,[1] A. Beck,[7] P. Bertin,[8] F. Butaru,[9] W. Boeglin,[10] A. Camsonne,[8] G. D. Cates,[3] C. C. Chang,[11] Seonho Choi,[9] E. Chudakov,[2] L. Coman,[10] J. C Cornejo,[6] B. Craver,[3] F. Cusanno,[12] R. De Leo,[13] C. W. de Jager†,[2] J. D. Denton,[14] S. Dhamija,[15] R. Feuerbach,[2] J. M. Finn†,[1] S. Frullani†,[16,17] K. Fuoti,[1] H. Gao,[4] F. Garibaldi,[16,17] O. Gayou,[7] R. Gilman,[2,18] A. Glamazdin,[19] C. Glashausser,[18] J. Gomez,[2] J.-O. Hansen,[2] D. Hayes,[20] B. Hersman,[21] D. W. Higinbotham,[2] T. Holmstrom,[1,14] T. B. Humensky,[3] C. E. Hyde,[20] H. Ibrahim,[20,22] M. Iodice,[12] X. Jiang,[18] L. J. Kaufman,[23] A. Kelleher,[1] K. E. Keister,[1] W. Kim,[24] A. Kolarkar,[15] N. Kolb,[15] W. Korsch,[15] K. Kramer,[1,4] G. Kumbartzki,[18] L. Lagamba,[13] V. Lainé,[2,8] G. Laveissiere,[8] J. J. Lerose,[2] D. Lhuillier,[25] R. Lindgren,[3] N. Liyanage,[3,2] H.-J. Lu,[26] B. Ma,[7] D. J. Margaziotis,[6] P. Markowitz,[10] K. McCormick,[18] M. Meziane,[4] Z.-E. Meziani,[9] R. Michaels,[2] B. Moffit,[1] P. Monaghan,[7] S. Nanda,[2] J. Niedziela,[23] M. Niskin,[10] R. Pandolfi,[27] K. D. Paschke,[23] M. Potokar,[28] A. Puckett,[3] V. A. Punjabi,[29] Y. Qiang,[7] R. Ransome,[18] B. Reitz,[2] R. Roché,[30] A. Saha†,[2] A. Shabetai,[18] S. Širca,[28] K. Slifer,[9] R. Snyder,[3] P. Solvignon†,[9] R. Stringer,[4] R. Subedi,[31] W. A. Tobias,[3] N. Ton,[3] P. E. Ulmer,[20] G. M. Urciuoli,[12] A. Vacheret,[25] E. Voutier,[32] K. Wang,[3] L. Wan,[7] B. Wojtsekhowski,[33] S. Woo,[24] H. Yao,[9] J. Yuan,[18] X. Zhan,[7] X. Zheng,[34] and L. Zhu[7]

(Jefferson Lab E97-110 Collaboration)

[1] *College of William and Mary, Williamsburg, Virginia 23187-8795, USA*
[2] *Thomas Jefferson National Accelerator Facility, Newport News, Virginia 23606, USA*
[3] *University of Virginia, Charlottesville, Virginia 22904, USA*
[4] *Duke University, Durham, North Carolina 27708, USA*
[5] *Yerevan Physics Institute, Yerevan 375036, Armenia*
[6] *California State University, Los Angeles, Los Angeles, California 90032, USA*
[7] *Massachusetts Institute of Technology, Cambridge, Massachusetts 02139, USA*
[8] *LPC Clermont-Ferrand, Université Blaise Pascal, CNRS/IN2P3, F-63177 Aubière, France*
[9] *Temple University, Philadelphia, Pennsylvania 19122, USA*
[10] *Florida International University, Miami, Florida 33199, USA*
[11] *University of Maryland, College Park, Maryland 20742, USA*
[12] *Istituto Nazionale di Fisica Nucleare, Sezione di Roma, Piazzale A. Moro 2, I-00185 Rome, Italy*
[13] *Istituto Nazionale di Fisica Nucleare, Sezione di Bari and University of Bari, I-70126 Bari, Italy*
[14] *Longwood University, Farmville, VA 23909, USA*
[15] *University of Kentucky, Lexington, Kentucky 40506, USA*
[16] *Istituto Nazionale di Fisica Nucleare, Sezione di Roma, I-00185 Rome, Italy*
[17] *Istituto Superiore di Sanità, I-00161 Rome, Italy*
[18] *Rutgers, The State University of New Jersey, Piscataway, New Jersey 08855, USA*
[19] *Kharkov Institute of Physics and Technology, Kharkov 310108, Ukraine*
[20] *Old Dominion University, Norfolk, Virginia 23529, USA*
[21] *University of New Hampshire, Durham, New Hamphsire 03824, USA*
[22] *Cairo University, Cairo, Giza 12613, Egypt*
[23] *University of Massachusetts-Amherst, Amherst, Massachusetts 01003, USA*
[24] *Kyungpook National University, Taegu City, South Korea*
[25] *DAPNIA/SPhN, CEA Saclay, F-91191 Gif-sur-Yvette, France*
[26] *Department of Modern Physics, University of Science and Technology of China, Hefei 230026, China*
[27] *Randolph-Macon College, Ashland, Virginia 23005, USA*
[28] *Institut Jozef Stefan, University of Ljubljana, Ljubljana, Slovenia*
[29] *Norfolk State University, Norfolk, Virginia 23504, USA*
[30] *Florida State University, Tallahassee, Florida 32306, USA*
[31] *Kent State University, Kent, Ohio 44242, USA*
[32] *LPSC, Université Joseph Fourier, CNRS/IN2P3, INPG, F-38026 Grenoble, France*
[33] *Thomas Jefferson National Accelerator Facility, Newport News, Virginia 23606, USA*
[34] *Argonne National Laboratory, Argonne, Illinois 60439, USA*

(Dated: August 13, 2019)

The spin-structure functions g_1 and g_2, and the spin-dependent partial cross-section σ_{TT} have been extracted from the polarized cross-sections differences, $\Delta\sigma_{\parallel}(\nu, Q^2)$ and $\Delta\sigma_{\perp}(\nu, Q^2)$ measured for the $^3\vec{\mathrm{He}}(\vec{\mathrm{e}}, \mathrm{e}')\mathrm{X}$ reaction at Jefferson Lab. Polarized electrons with energies from 1.147 to 4.404 GeV were scattered at angles of 6° and 9° from a longitudinally or transversely polarized ^{3}He target. The data cover the kinematic regions of the quasi-elastic, resonance and beyond. From the extracted spin-structure functions, the first moments $\overline{\Gamma_1}(Q^2)$, $\Gamma_2(Q^2)$ and $I_{\rm TT}(Q^2)$ are evaluated with high precision for the neutron in the Q^2 range from 0.035 to 0.24 GeV^2. Finally, these low Q^2 results are used to test chiral perturbation theory calculations.

The study of nucleon spin structure has been actively pursued over the past thirty years, both experimentally and theoretically [1]. It provides a powerful means to study quantum chromodynamics (QCD), the gauge theory of strong interactions. In particular, moments of the spin structure functions provide an opportunity to study QCD throughout its different regimes by comparing measurements of these observables to QCD-based calculations. This includes the low momentum regime where calculations are difficult due to the increasingly large coupling of QCD [2]. In this non-perturbative region, effective field theories derived from QCD, such as chiral effective field theory (χEFT) [3], are used.

Spin-dependent sum rules are important tools to study nucleon spin structure. A sum rule of great interest is the one of Gerasimov, Drell, and Hearn (GDH) [4]. It links an integral over the excitation spectrum of the helicity-dependent photoabsorption cross-sections to the target's anomalous magnetic moment κ. The sum rule stems from causality, unitarity, and Lorentz and gauge invariances. Its expression for a spin-$\frac{1}{2}$ target is:

$$\int_{\nu_0}^{\infty} \left[\sigma_{\frac{1}{2}}(\nu) - \sigma_{\frac{3}{2}}(\nu)\right] \frac{d\nu}{\nu} = -\frac{2\pi^2\alpha}{M_t^2}\kappa^2, \qquad (1)$$

where M_t is the target mass, ν the photon energy, ν_0 the inelastic threshold and α is the fine-structure constant. The $\frac{1}{2}$ ($\frac{3}{2}$) indicates that the photon helicity is parallel (anti-parallel) to the target spin. The GDH sum rule can be applied to various targets such as ^{3}He and the neutron, with predictions of -498.0 and -232.5 μb, respectively.

Starting in the 1980's, generalizations of the integrand for virtual photon absorption were proposed [5–7], e.g.:

$$I_{\rm TT}(Q^2) \equiv \frac{M_t^2}{4\pi^2\alpha}\int_{\nu_0}^{\infty}\frac{\kappa_f(\nu,Q^2)}{\nu}\frac{\sigma_{1/2}(\nu,Q^2)-\sigma_{3/2}(\nu,Q^2)}{\nu}d\nu$$
$$= \frac{2M_t^2}{Q^2}\int_0^{x_0}\left[g_1(x,Q^2) - \frac{4M_t^2}{Q^2}x^2 g_2(x,Q^2)\right]dx, \qquad (2)$$

where ν is the energy transfer, Q^2 the four-momentum transfer squared, κ_f the virtual photon flux, $x = \frac{Q^2}{2M_t\nu}$ is the Bjorken scaling variable, $x_0 = \frac{Q^2}{2M_t\nu_0}$, and g_1 and g_2 are the spin structure functions. These relations extend the sum rule to electron scattering. The sum rule itself was generalized by Ji and Osborne [8] using a dispersion relation involving the forward virtual Compton scattering amplitude in the $\nu \to 0$ limit, $S_1(0, Q^2)$:

$$\overline{\Gamma_1}\left(Q^2\right) \equiv \int_0^{x_0} g_1(x,Q^2)dx = \frac{Q^2}{8}\overline{S_1}(0,Q^2)\,, \qquad (3)$$

where the bar indicates exclusion of the elastic contribution. This relation, valid at any Q^2, can be applied back to Eq. (2), equating the moment $I_{TT}(Q^2)$ to $A_{TT}(0,Q^2)$, the spin-flip VVCS amplitude in the $\nu \to 0$ limit. Eqs. (2) or (3) can then be used to compare theoretical methods relevant at a given Q^2 and experimental data. Earlier data [9–13] taken at intermediate Q^2 revealed tensions with the then available χEFT calculations of $\overline{S_1}(0,Q^2)$ and $A_{TT}(0,Q^2)$ [14, 15], even for the lowest Q^2 experimentally covered [1]. The discrepancies between data and calculations can be due to the Q^2 coverage of the experiments being not low enough for a valid comparison with χEFT, and/or to the calculations themselves. The data, particularly that of E94-010 [10–12], underlined the importance of treating properly the $\Delta(1232)$ resonance in the χEFT calculations. The data also showed the need for measuring spin moments at Q^2 low enough so that χEFT calculations can be accurately tested. We report here on such data for the neutron.

The other spin structure function g_2 is expected to obey the Burkhardt–Cottingham (BC) sum rule [16]:

$$\Gamma_2(Q^2) \equiv \int_0^1 g_2(x,Q^2)dx = 0\,, \qquad (4)$$

a super-convergence relation, i.e. implicitly independent of Q^2, derived from the dispersion relation for the Compton scattering amplitude $S_2\left(Q^2\right)$ [6]. The BC sum rule's validity depends on the convergence of the integral and assumes that g_2 is well-behaved as $x \to 0$ [17].

We present here data on g_1, g_2 and $\sigma_{\rm TT} \equiv (\sigma_{\frac{1}{2}} - \sigma_{\frac{3}{2}})/2$ on ^{3}He, and of $\overline{\Gamma_1}$, Γ_2 and $I_{\rm TT}$ for the neutron, for $0.035 \leq Q^2 \leq 0.24$ GeV^2. They provide a benchmark test of χEFT calculations.

Experiment E97-110 [18, 19] acquired data in Hall A [20] at Jefferson Lab (JLab). We measured the inclusive reaction $^3\vec{\rm He}(\vec{\rm e},{\rm e}')$ with a longitudinally polarized electron beam scattered from longitudinally or transversely (in-plane) polarized ^{3}He [20]. Eight beam energies E and two scattering angles θ were used to cover kinematics at constant Q^2, see Fig. 1. The data cover invariant mass $W = \sqrt{M^2 + 2M\nu - Q^2}$ (M is the nucleon mass) values from the elastic up to 2.5 GeV; however, only the results above the pion production threshold ($W = 1.073$ GeV) are discussed here. For the experiment, spin asymmetries and absolute cross-sections were both measured. The beam polarization was flipped

*Contact author. Email: deurpam@jlab.org
†Deceased.

pseudo-randomly at 30 Hz and Møller and Compton polarimeters [20] measured it to average at 75.0 ± 2.3%. The beam current ranged from 1 to 10 μA depending on the trigger rate. The data acquisition rate was limited to 4 kHz to keep the deadtime below 20%.

The ^{3}He target was polarized by spin-exchange optical pumping (SEOP) [21]. Two sets of Helmholtz coils providing a parallel or transverse 2.5 mT uniform field allowed us to orient the ^{3}He spins longitudinally or perpendicularly to the beam direction. The target had about 12 atm of ^{3}He gas in a glass cell consisting of two connected chambers. The SEOP process occurred in the upper chamber, which was illuminated with 90 W of laser light at a wavelength of 795 nm. The electron beam passed through a lower chamber made of a 40 cm-long cylinder with a diameter of 2 cm and hemispherical glass windows at both ends. Two independent polarimetries monitored the ^{3}He polarization: nuclear magnetic resonance (NMR) and electron paramagnetic resonance (EPR). The NMR system was calibrated using adiabatic fast passage and the known thermal equilibrium polarization of water. The polarization was independently cross-checked by measuring the elastic ^{3}He asymmetry. The average in-beam target polarization was (39.0 ± 1.6)%.

The scattered electrons were detected by a High Resolution Spectrometer (HRS) [20] with a lowest scattering angle reachable of 12.5°. A horizontally-bending dipole magnet [22] was placed in front of the HRS so that electrons with scattering angles of 6° or 9° could be detected. The HRS detector package consisted of a pair of drift chambers for tracking, a pair of scintillator planes for triggering and a gas Cherenkov counter, together with a two layer electromagnetic calorimeter for particle identification. Details of the experimental set-up and its performance can be found in [18, 19].

The g_1 and g_2 spin structure functions were extracted from the cross-section differences $\Delta\sigma_\parallel \equiv \frac{d^2\sigma^{\downarrow\Uparrow}}{d\Omega dE'} - \frac{d^2\sigma^{\uparrow\Uparrow}}{d\Omega dE'}$ and $\Delta\sigma_\perp \equiv \frac{d^2\sigma^{\downarrow\Rightarrow}}{d\Omega dE'} - \frac{d^2\sigma^{\uparrow\Rightarrow}}{d\Omega dE'}$ for the case where the target polarization is aligned parallel or perpendicular, respectively, to the beam direction:

$$g_1 = \frac{MQ^2\nu}{4\alpha^2}\frac{E}{E'}\frac{1}{E+E'}\left[\Delta\sigma_\parallel + \tan\left(\frac{\theta}{2}\right)\Delta\sigma_\perp\right]$$
$$g_2 = \frac{MQ^2\nu}{8\alpha^2 E'(E+E')}\left[-\Delta\sigma_\parallel + \frac{E+E'\cos\,\theta}{E'\sin\,\theta}\Delta\sigma_\perp\right].$$

The cross-section differences $\Delta\sigma_{\parallel,\perp}$ were formed by combining longitudinal and transverse asymmetries $A_\parallel$ and $A_\perp$ with the unpolarized absolute cross-section σ_0: $\Delta\sigma_{\parallel,\perp} = 2\sigma_0 A_{\parallel,\perp}$. Unpolarized backgrounds cancel in $\Delta\sigma$. The physics asymmetries were obtained by correcting the raw asymmetries for the beam and target polarizations, as well as beam charge and data acquisition lifetime asymmetries.

The absolute cross-section was obtained by correcting for the finite HRS acceptance and detector inefficiencies. The $1/\nu$ weighting of the GDH sum emphasizes low ν contributions. Thus, contamination from elastic and quasi-elastic events appearing beyond the electroproduction threshold due to detector resolution and radiative tails was carefully studied and corrected on both σ_0 and $\Delta\sigma_{\parallel,\perp}$. The high HRS momentum resolution helped to minimize the contamination. For the neutron moments, the quasi-elastic contamination was studied and subtracted by building a model of our data with guidance from state-of-the-art Faddeev calculations [23] and the MAID [24] model. The estimated uncertainty from the subtraction and the effect of varying the lower limit of integration (to account for below-threshold pion production) were included in our systematic uncertainty. Since g_1 and g_2 are defined in the Born approximation, radiative corrections were applied following Ref. [25] for the unpolarized case and using Ref. [26] to include polarized effects. Our data were used in that procedure, to reduce the systematic uncertainty.

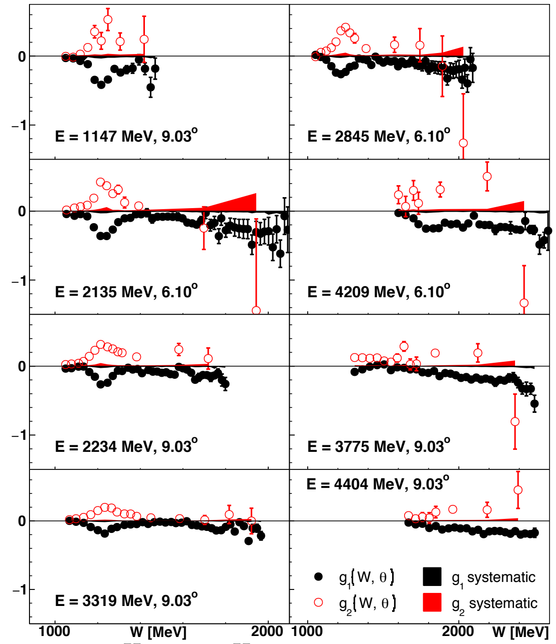

FIG. 1: $g_1^{^3\mathrm{He}}$ and $g_2^{^3\mathrm{He}}$ at fixed θ and E, versus W.

The results for g_1 and g_2, and for σ_{TT} on ^{3}He are shown in Fig. 1 and Fig. 2, respectively. The Hand convention, $\kappa_f = \nu - Q^2/(2M)$, was used to form σ_{TT}. The data are provided from the pion threshold. The error bars represent the statistical uncertainty. Systematic uncertainties are shown by the lower band for g_1 and σ_{TT} or the upper band for g_2. The main systematic uncertainties are from the absolute cross-sections (3.5 to 4.5%), beam polarization (3.5%), target polarization (3 to 5%) and radiative corrections (3 to 7%). The data display a prominent feature in the $\Delta(1232)$ region. There, $g_1 \approx -g_2$. This is expected, since the Δ is an $M1$ resonance for which the longitudinal-transverse interference cross-section $\sigma'_{\mathrm{LT}} \propto (g_1 + g_2)$ is anticipated to be highly suppressed [7]. Above the Δ, both spin struc-

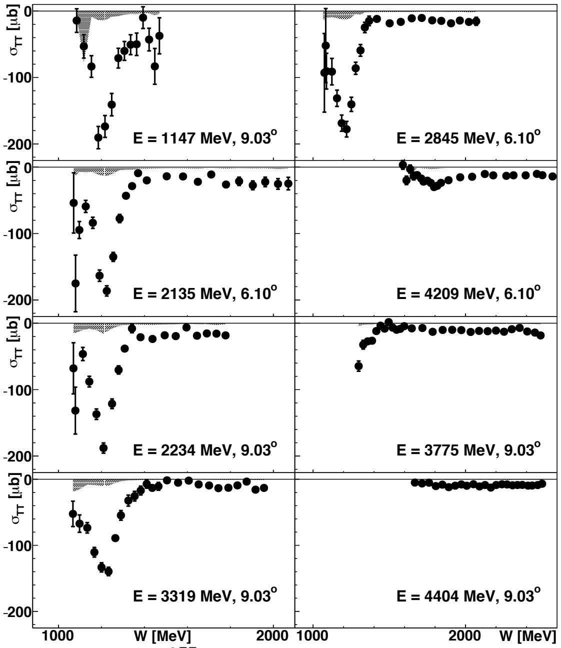

FIG. 2: $\sigma_{\mathrm{TT}}^{^3\mathrm{He}}$ at fixed θ and E, versus W.

ture functions decrease in magnitude, to increase again as W approaches 2 GeV while still displaying an approximate symmetry indicating the smallness of σ'_{LT} or, at the larger Q^2 values, the smallness of higher-twist effects.

To obtain $\overline{\Gamma_1}$, $\overline{\Gamma_2}$ and I_{TT}, g_1, g_2 and σ_{TT} were evaluated at constant Q^2 by interpolating the fixed θ and E data. The moments were then formed for each value of Q^2 with integration limits from pion threshold to W between 2 to 2.5 GeV, depending on the Q^2. The neutron moments were obtained using the prescription in Ref. [27] which treats the polarized ^{3}He nucleus as an effective polarized neutron. The uncertainty on the method was estimated to be 5 to 10% for $Q^2 \leq 0.25$ GeV^2 from their model calculation. The same neutron parameterization as in a previous JLab experiment [28] was used to complete the integration down to $x = 0.001$, and the recent Regge parameterization of Ref. [29] was used for $x < 0.001$. Results for the integrals are given in Table I.

In Fig. 3 our $\overline{\Gamma_1^n}$ is compared to χEFT calculations [31, 32], models [33, 34], the MAID parameterization [24] which contains only resonance contributions, and earlier data [9, 11, 30]. Where the Q^2 coverages overlap, our data agree with the earlier data extracted either from the deuteron or ^{3}He. Our precision is much improved compared to the EG1 data and similar to that of the E94-010 data at larger Q^2.

Two χEFT calculations have become available recently [31, 32], improving on the earlier ones [14, 15]. Those had used different approaches, and different ways to treat for the $\Delta(1232)$ degree of freedom, a critical component of χEFT calculations for baryons. The two state-of-art calculations [31, 32] account explicitly for the Δ by computing the $\pi - \Delta$ graphs, but differ in their expansion methods for these corrections. In χEFT, the general

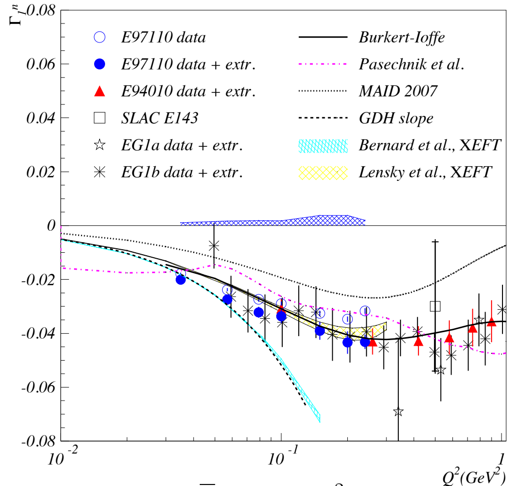

FIG. 3: The neutron $\overline{\Gamma}_1$ versus Q^2 from this experiment (E97-110), compared to the world data and models. The filled circles show the full integral from E97-110 with the estimated unmeasured low-x contribution. The open circles show the measured partial integral. The inner error bars on the E97-110 and E94-010 points, often too small to be visible, represent the statistical uncertainties. The combined statistical and uncorrelated systematic uncertainties are shown by the outer error bars. The correlated systematic uncertainty is indicated by the band. The GDH sum rule provides $d\overline{\Gamma}_1/dQ^2$ at $Q^2 = 0$ (dashed line), see Eqs. 2 or 3.

expansion parameter is $m_\pi/\Lambda_{\chi\mathrm{SB}}$ where m_π is the pion mass and $\Lambda_{\chi\mathrm{SB}} \approx 1$ GeV is the chiral symmetry breaking scale. To explicitly account for the Δ degree of freedom, the nucleon-Δ mass gap $m_{N\Delta}$ needs to be included in the chiral expansion. Ref. [31] treats $m_{N\Delta}$ as a small parameter of the same order as m_π. Ref. [32] uses $m_{N\Delta}$ as an intermediate scale so that $m_{N\Delta}/\Lambda_{\chi\mathrm{SB}} \approx m_\pi/m_{N\Delta}$ is the expansion parameter for the π-Δ corrections. Our $\overline{\Gamma}_1^n$ data agree with these calculations up to $Q^2 \approx 0.1$ GeV^2 and then agree only with calculation [32], which predicts the plateauing of the data. The deviation for $Q^2 \gtrsim 0.1$ GeV^2 between data and the calculation from Ref. [31] is expected since, as pointed out in [31], a similar deviation is seen with proton data but not for the isovector quantity $\Gamma_1^{(p-n)}$ [13]. The issue thus affects isoscalar combinations and can be traced to the later onset of loop contributions for isoscalar quantities (3 pions, in contrast with 2 pions threshold to isoscalar quantities) [31].

$I_{\mathrm{TT}}^n(Q^2)$ is shown in Fig. 4. The integration using only our data, and that with an estimate of the unmeasured low-x part are represented by the open and solid circles, respectively. The measured integral should be compared to the MAID result (solid line), which is less negative than the data. Our data and the earlier data [10] are consistent over their overlap region. As Q^2 decreases, our results drop to around -325 μb, agreeing with the χEFT calculation from Bernard *et al.* [31]. The calculation from Lensky *et al.* [32] displays the same Q^2-dependence as the data but with a systematic shift.

$\Gamma_2^n\left(Q^2\right)$ is shown in Fig. 5. The stars show the mea-

Q^2 [GeV]^2	$\Gamma_1^{n,\ data}$	$\Gamma_1^{n,\ data+extr.}$	stat.	$I_{\rm TT}^{n,\ data}$[μb]	$I_{\rm TT}^{n,\ data+extr.}$[$\mu$b]	stat.[μb]
0.035	$(-1.78 \pm 0.18(\text{syst.})) \times 10^{-2}$	$(-2.01 \pm 0.18(\text{syst.})) \times 10^{-2}$	4×10^{-4}	-293 ± 25	-322 ± 25	8
0.057	$(-2.38 \pm 0.23(\text{syst.})) \times 10^{-2}$	$(-2.74 \pm 0.23(\text{syst.})) \times 10^{-2}$	6×10^{-4}	-296 ± 24	-324 ± 24	8
0.079	$(-2.73 \pm 0.27(\text{syst.})) \times 10^{-2}$	$(-3.22 \pm 0.28(\text{syst.})) \times 10^{-2}$	10×10^{-4}	-284 ± 26	-312 ± 26	11
0.100	$(-2.89 \pm 0.30(\text{syst.})) \times 10^{-2}$	$(-3.36 \pm 0.31(\text{syst.})) \times 10^{-2}$	8×10^{-4}	-252 ± 21	-274 ± 21	7
0.150	$(-3.26 \pm 0.49(\text{syst.})) \times 10^{-2}$	$(-3.91 \pm 0.50(\text{syst.})) \times 10^{-2}$	10×10^{-4}	-202 ± 18	-221 ± 18	6
0.200	$(-3.47 \pm 0.55(\text{syst.})) \times 10^{-2}$	$(-4.34 \pm 0.56(\text{syst.})) \times 10^{-2}$	10×10^{-4}	-168 ± 11	-187 ± 12	4
0.240	$(-3.17 \pm 0.30(\text{syst.})) \times 10^{-2}$	$(-4.31 \pm 0.32(\text{syst.})) \times 10^{-2}$	10×10^{-4}	-144 ± 10	-165 ± 10	4

TABLE I: Measured GDH integrals. From left to right: Four-momentum transfer; Γ_1^n measured up to a W between 2 to 2.5 GeV, depending on the Q^2; full Γ_1^n with low-x (equivalently large-W) extrapolation; statistical uncertainty on Γ_1^n; measured $I_{\rm TT}^n$; full $I_{\rm TT}^n$; statistical uncertainty on $I_{\rm TT}^n$. Systematic uncertainties have been added in quadrature.

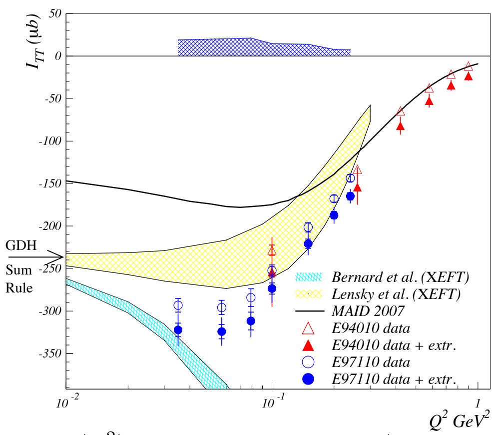

FIG. 4: $I_{\rm TT}(Q^2)$ for the neutron, with (filled circles) and without (open circles) the estimated unmeasured low-x contribution. The meaning of the inner and outer error bars and of the band is the same as in Fig. 3. Also shown are χEFT results, MAID (solid line) and earlier JLab data [10].

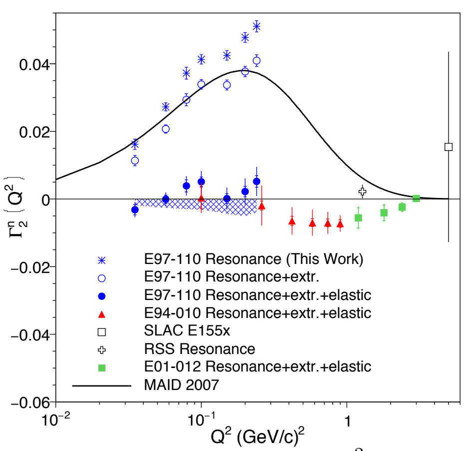

FIG. 5: The neutron Γ_2 data versus Q^2. The error band represents the correlated systematic uncertainty from radiative corrections, interpolation of g_2 to constant Q^2, model uncertainties in the neutron extraction from ^{3}He, and the elastic contribution uncertainty. The uncorrelated systematic and statistical uncertainties added in quadrature are shown by the outer error bars. The inner error bars (when visible) represent the statistical uncertainty. Also shown is the MAID model with only resonance contributions.

sured integral without low-x extrapolation for the neutron, to be compared with MAID. This one underestimates the higher Q^2 data but agrees well at lower Q^2. The open circles represent the integral including an estimate for the low-x contribution assuming $g_2 = g_2^{WW}$ [37], where g_2^{WW} is the twist-2 part of g_2 [35]. This procedure is used since there are little data to constrain g_2 at low-x. Since it is unknown how well g_2^{WW} matches g_2 there, one cannot reliably assess an uncertainty on the $W > 2$ GeV extrapolation and none was assigned. The solid circles show the full integral with the elastic contribution evaluated using Ref. [36]. These data allow us to investigate the BC sum rule in this low-Q^2 region with the caveat of the unknown uncertainty attached to the low-x extrapolation. Under this provision, the data are consistent with the sum rule expectation that $\Gamma_2 = 0$ for all Q^2. They also agree with the earlier results from E94-010 (triangles). Higher Q^2 data from E01-012 (filled squares) [38], RSS (open crosses) [39], and E155x (open square) [37] are also consistent with zero.

In conclusion, ^{3}He spin structure functions $g_1(\nu, Q^2)$, $g_2(\nu, Q^2)$ and the spin-dependent partial cross-section $\sigma_{\rm TT}(\nu, Q^2)$ were measured at low Q^2. The moments $\overline{\Gamma_1}(Q^2)$, $\Gamma_2(Q^2)$ and $I_{\rm TT}(Q^2)$ of the neutron are extracted at $0.035 \le Q^2 \le 0.24$ GeV^2. They are compared to two next-to-leading-order χEFT calculations from two separate groups, Bernard *et al.* [31] and Lensky *et al.* calculation [32]. The $\overline{\Gamma}_1(Q^2)$ and $I_{\rm TT}(Q^2)$ integrals agree with published data at higher Q^2. The data on $\overline{\Gamma_1}$ agree reasonably with both recent χEFT calculations. The data on $I_{\rm TT}$ disagree with the calculation [32] and that of [31] except at the lowest Q^2 point. That the results for two recent χEFT methods differ, and that they describe with different degrees of success the data underlines the importance of the Δ degree of freedom for spin observables and the sensitivity of χEFT to the consequent π-Δ terms. The earlier E94-010 data had triggered improvement of the χEFT calculations. Now, the precise E97-110 data, taken in the chiral domain, show that yet further sophistication of χEFT is needed before spin observables can be satisfactorily described. Our determination of $\Gamma_2^n(Q^2)$ agrees with the BC sum rule in this low-Q^2 region, with the proviso that g_2^{ww} is used to assess the unmeasured low-x part of Γ_2. Analysis of data down to $Q^2 = 0.02$ GeV^2 taken at a different time under different conditions, which requires a different analysis, is currently ongoing. These data and results on $\sigma'_{\rm LT}$, the spin polarizabilities γ_0^n and $\delta_{\rm LT}^n$, and moments for ^{3}He will be reported in future publications. All these data, when combined with results [28] obtained on deuteron and future proton data [40] taken at low Q^2, will yield further extensive tests of calculations from χEFT, the leading effective theory of strong interactions at low Q^2.

We acknowledge the outstanding support of the Jefferson Lab Hall A technical staff and the Physics and Accelerator Divisions that made this work possible. We thank A. Deltuva, J. Golak, F. Hagelstein, H. Krebs, V. Lensky, U.-G. Meißner, V. Pascalutsa, G. Salmè, S. Scopetta and M. Vanderhaeghen for useful discussions and for sharing their calculations. This material is based upon work supported by the U.S. Department of Energy, Office of Science, Office of Nuclear Physics under contract DE-AC05-06OR23177, and by the NSF under grant PHY-0099557.

[1] J. P. Chen, A. Deur and Z. E. Meziani, Mod. Phys. Lett. A **20**, 2745 (2005) J. P. Chen, Int. J. Mod. Phys. E **19**, 1893 (2010) S. E. Kuhn, J.-P. Chen and E. Leader, Prog. Part. Nucl. Phys. **63**, 1 (2009) A. Deur, S. J. Brodsky and G. F. De Téramond, Rep. Prog. Phys., **82**, 7 (2019)

[2] A. Deur, S. J. Brodsky and G. F. de Teramond, Prog. Part. Nucl. Phys. **90**, 1 (2016)

[3] V. Bernard, N. Kaiser and U. G. Meissner, Int. J. Mod. Phys. E **4**, 193 (1995)

[4] S. B. Gerasimov, Sov. J. Nucl. Phys. **2**, 430 (1966) [Yad. Fiz. **2**, 598 (1965)]; S. D. Drell and A. C. Hearn, Phys. Rev. Lett. **16**, 908 (1966); M. Hosoda and K. Yamamoto Prog. Theor. Phys. 36 (2), 425 (1966)

[5] M. Anselmino, B. L. Ioffe and E. Leader, Sov. J. Nucl. Phys. **49**, 136 (1989) [Yad. Fiz. **49**, 214 (1989)]

[6] D. Drechsel, B. Pasquini and M. Vanderhaeghen, Phys. Rept. **378**, 99 (2003)

[7] D. Drechsel, S. S. Kamalov and L. Tiator, Phys. Rev. D **63**, 114010 (2001)

[8] X. D. Ji and J. Osborne, J. Phys. G **27**, 127 (2001)

[9] J. Yun *et al.*, [EG1a experiment] Phys. Rev. C **67**, 055204 (2003); K. Slifer *et al.*, [E94-010 experiment] Phys. Rev. Lett. **101**, 022303 (2008); N. Guler *et al.*, [EG1b experiment] Phys. Rev. C **92**, no. 5, 055201 (2015); R. Fersch *et al.*, [EG1b experiment] Phys. Rev. C **96**, no. 6, 065208 (2017)

[10] M. Amarian *et al.*, [E94-010 experiment] Phys. Rev. Lett. **89**, 242301 (2002)

[11] M. Amarian *et al.*, [E94-010 experiment] Phys. Rev. Lett. **92**, 022301 (2004)

[12] M. Amarian *et al.*, [E94-010 experiment] Phys. Rev. Lett. **93**, 152301 (2004)

[13] A. Deur *et al.*, Phys. Rev. Lett. **93**, 212001 (2004); Phys. Rev. D **78**, 032001 (2008); Phys. Rev. D **90**, no. 1, 012009 (2014)

[14] V. Bernard, T. R. Hemmert and U. G. Meissner, Phys. Rev. D **67**, 076008 (2003)

[15] X. D. Ji, C. W. Kao and J. Osborne, Phys. Lett. B **472**, 1 (2000)

[16] H. Burkhardt and W. N. Cottingham, Annals Phys. **56**, 453 (1970)

[17] R. L. Jaffe and X. D. Ji, Phys. Rev. D **43**, 724 (1991)

[18] V. Sulkosky Ph.D. thesis, Col. of William & Mary (2007)

[19] Details of JLab E97110 and relevant theses can be found at http://hallaweb.jlab.org/experiment/E97-110/

[20] J. Alcorn *et al.*, Nucl. Instrum. Meth. A **522**, 294 (2004)

[21] T. R. Gentile, P. J. Nacher, B. Saam and T. G. Walker, Rev. Mod. Phys. **89**, no. 4, 045004 (2017)

[22] F. Garibaldi *et al.* Phys. Rev. C **99**, no. 5, 054309 (2019)

[23] J. Golak, *et al.*, Phys. Rev. C **65**, 064004 (2002); Phys. Rev. C **72**, 054005 (2005); L. P. Yuan, *et al.*, Phys. Rev. C **66**, 054004 (2002); A. Deltuva, *et al.*, Phys. Rev. C **69**, 034004 (2004); Phys. Rev. C **70**, 034004 (2004); Phys. Rev. C **71**, 054005 (2005)

[24] D. Drechsel, O. Hanstein, S. S. Kamalov and L. Tiator, Nucl. Phys. A **645**, 145 (1999)

[25] L. W. Mo and Y. S. Tsai, Rev. Mod. Phys. **41**, 205 (1969)

[26] I. V. Akushevich and N. M. Shumeiko, J. Phys. G **20**, 513 (1994); I. Akushevich, A. Ilyichev, N. Shumeiko, A. Soroko and A. Tolkachev, Comput. Phys. Commun. **104**, 201 (1997)

[27] C. Ciofi degli Atti and S. Scopetta, Phys. Lett. B **404**, 223 (1997)

[28] K. P. Adhikari *et al.*, [EG4 experiment] Phys. Rev. Lett. **120**, no. 6, 062501 (2018)

[29] S. D. Bass, M. Skurzok and P. Moskal, Phys. Rev. C **98**, no. 2, 025209 (2018)

[30] P. L. Anthony *et al.*, [E142 experiment] Phys. Rev. D **54**, 6620 (1996); K. Abe *et al.*, [E143 experiment] Phys. Rev. D **58**, 112003 (1998); K. Abe *et al.*, [E154 experiment] Phys. Rev. Lett. **79**, 26 (1997)

[31] V. Bernard, E. Epelbaum, H. Krebs and U. G. Meissner, Phys. Rev. D **87**, no. 5, 054032 (2013)

[32] V. Lensky, J. M. Alarcón and V. Pascalutsa, Phys. Rev. C **90**, no. 5, 055202 (2014). 2019 update: private communication.

[33] V. D. Burkert and B. L. Ioffe, Phys. Lett. B **296**, 223 (1992); J. Exp. Theor. Phys. **78**, 619 (1994) [Zh. Eksp. Teor. Fiz. **105**, 1153 (1994)]

[34] R. S. Pasechnik, J. Soffer and O. V. Teryaev, Phys. Rev. D **82**, 076007 (2010); R. S. Pasechnik, D. V. Shirkov, O. V. Teryaev, O. P. Solovtsova and V. L. Khandramai, Phys. Rev. D **81**, 016010 (2010)

[35] S. Wandzura and F. Wilczek, Phys. Lett. B **72**, 195 (1977)

[36] P. Mergell, U. G. Meissner and D. Drechsel, Nucl. Phys. A **596**, 367 (1996)

[37] P. L. Anthony *et al.*, [E155x experiment] Phys. Lett. B **553**, 18 (2003)

[38] P. Solvignon *et al.*, [E01-012 experiment] Phys. Rev. C **92**, 015208 (2015)

[39] K. Slifer *et al.*, [RSS experiment] Phys. Rev. Lett. **105**, 101601 (2010)

[40] M. Battaglieri, R. De Vita, A. Deur and M. Ripani, spokespersons for Jefferson Lab Experiment E03-006 (2003); A. Camsonne, J.-P. Chen and K. Slifer, spokespersons for Jefferson Lab Experiment E08-027 (2008)